Vietnam Journal of Catalysis and Adsorption
Tạp chí xúc tác và hấp phụ Việt Nam

https://jca.edu.vn

Low-Temperature Catalytic Oxidation of Volatile Organic Compounds (VOCs) using Transition Metal Mixed Oxide Catalysts

Nguyen Khac Tuan[1], Duong Hoang Anh[1], Ta Dinh Quang[1], Le Minh Thang[1,*]

[1] *School of Chemistry and Life Science, Hanoi University of Science and Technology, Hanoi, Vietnam*
**Email: thang.leminh@hust.edu.vn*

ARTICLE INFO

Received: 09/6/2024
Accepted: 18/6/2024
Published: 30/06/2024

Keywords:
Cu-Mn composite oxide, Toluene, Benzene lattice oxygen mobility

ABSTRACT

This work investigated the modification of MnO_x catalysts by doping various metals (e.g., Cu) and supporting them on cordierite honeycomb ceramics using the impregnation method. The catalysts were characterized by BET, XRD, SEM-EDX, and H_2-TPR techniques. The $Cu_1Mn_2O_x$ catalyst exhibited the best catalytic performance, achieving complete oxidation of benzene and toluene at 275°C with a WHSV of 18,000 mL/(g·h). The excellent performance was attributed to the formation of a Cu-Mn solid solution with a spinel structure, which increased adsorbed oxygen species and enhanced lattice oxygen mobility. This improved catalyst reducibility and oxygen species activity, as demonstrated by significantly lower reduction temperatures of Cu-Mn composite oxides through H_2-TPR. The monolithic $Cu_1Mn_2O_x$ catalyst showed good stability over 16 hours of testing and excellent cycle ability, indicating great potential for practical application.

1. Introduction

Volatile organic compounds (VOCs) are identified as major pollutants, detrimental to both the environment and human health. Consequently, effective technologies/methods for VOCs removal are essential to safeguard human health and mitigate environmental pollution [1]. Currently, numerous approaches are being researched and developed for VOCs elimination, among which low-temperature catalytic oxidation and adsorption are gaining increasing attention due to their advantages such as low operating temperatures and reduced emission of harmful byproducts [2]. Adsorption, in particular, is easy to implement and offers high removal efficiency. Presently, highly active noble metal catalysts are being utilized for low-temperature s oxidation [3]. However, despite their high activity, they are expensive, prone to poisoning, and susceptible to sintering during prolonged operation. Transition metal oxides like manganese oxide, cobalt oxide, and copper oxide, readily available in the market at relatively low cost, with superior thermal stability and poisoning resistance, are gradually garnering more interest [4]. Among these transition metal oxides, manganese oxide (MnO_x) has attracted significant research attention due to its potential for VOCs removal, owing to its diverse structure and multiple valence states [5]. However, the activity of single metal oxides at low temperatures is not high and requires improvement for catalytic VOC oxidation.

To enhance catalyst activity, various methods have been employed, with metal doping being one of the effective approaches to promote low-temperature catalytic activity. Research on modifying MnO_x by incorporating different cations such as Co-Mn, Fe-Mn,

https://doi.org/10.62239/jca.2024.041

and Cu-Mn has led to the formation n of mixed metal oxides [6-8], leveraging the synergistic effects between Mn and other metal cations. In this study, Cu-Mn oxide catalysts were synthesized and compared with pure single metal oxides CuO and MnO_2. To overcome the drawbacks of conventional powder catalysts (e.g., high-pressure drop, susceptibility to sintering, and low mechanical strength under high gas flow), cordierite ceramic, a common monolithic catalyst support, was employed due to its properties such as good thermal stability, mechanical stability, and coating adhesion [9]. The active phase components were loaded onto the cordierite ceramic support. The $CuMnO_x$ catalyst was synthesized using a simple and effective impregnation method, replacing complex multi-step and time-consuming synthesis methods like aluminum coating and hydrothermal techniques [10]. Various physicochemical characterizations, including XRD, BET, GC-TCD, TPR-H_2, and SEM-EDS, were conducted to investigate the catalysts.

2. Experimental

Preparation of catalysts

The $CuMnO_x$ oxide catalyst was synthesized via a wet impregnation method using cordierite ceramic as the support. Precursor salts $Cu(NO_3)_2.3H_2O$ and $Mn(NO_3)_2.4H_2O$ were dissolved in distilled water to achieve a molar ratio of Cu^{2+}:Mn^{2+} of 1:2. Citric acid solution was then added dropwise to the mixture. Cordierite ceramic was introduced into the solution for impregnation, which was conducted at 60℃ for 1 hour under continuous magnetic stirring. Subsequently, the impregnated ceramic was removed from the solution, dried at 120℃ for 30 minutes, and calcined at 300℃ for 45 minutes with a heating rate of 3℃/min. This impregnation process was repeated three times to optimize the loading of the active phase onto the support. Finally, the catalyst sample was calcined at 500℃ for 3 hours with a heating rate of 3℃/min.

Characterization of the Catalysts

The exterior surface mophology of the catalysts was determined by a scanning electron microscopy (SEM) (JEOL Benchtop SEM JCM-7000 NeoScope). The crystallinity of the catalysts was investigated by X-ray powder diffraction (XRD) using a Bruker Axs D8 Advance XRD diffractometer (Germany) with Cu Ka irradiation (40kV, 40 mA). The specific surface areas of the catalysts were determined by N_2 adsorption using a Micromeritics Gemini VII 2390 instrument, GeViCat center, Hanoi University of Science and Technology. The Autochem II 2920 device at GeViCat center, Hanoi University of Science and Technology was used to record H_2 -TPR profile.

Measurement of catalytic activity

Performance of catalysts was evaluated in a continuous-flow fixed-bed quartz microreactor (inner diameter 3 mm) at a space velocity (SV) of 18.000 mL/g.hr. Catalysts 200 mg were loaded in the quartz reactor with quartz wool packed at both ends of the catalyst bed. The continuous flow (60 mL/min) was composed of oxygen, nitrogen and toluene and benzene concentrations are 7000 ppm, 12000 ppm respectively. According to Eq. (1), the weight-hourly airspeed of the gas was 18,000 $mL{\cdot}g^{-1}{\cdot}h^{-1}$.

$$\mathrm{WHSV} = \frac{Q_{totalflow}}{m_{catalyst}} \quad (1)$$

The concentration of benzene, toluene and CO_2 in the effluent gas was analyzed by gas chromatograph - Thermo Focus (Italia) equipped with a thermal conductivity detector (TCD).

The conversion of toluene and benzene, along with the selectivity towards CO_2, were determined using equations (2) to (4). In which:

$$\eta_T = \frac{C_i^T - C_o^T}{C_i^T} \times 100\% \quad (2)$$

$$\gamma_{Benzene \rightarrow CO_2} = \frac{C^o_{CO_2,T}}{6 \times \left(C^i_T - C^o_T\right)} \times 100\% \quad (3)$$

$$\gamma_{Toluene \rightarrow CO_2} = \frac{C^o_{CO_2,T}}{7 \times \left(C^i_T - C^o_T\right)} \times 100\% \quad (4)$$

Where, η_T : VOC conversion (%);

C_i, C_o : VOC concentration of inlet and outlet flow at a temperature T (ppm);

γ : the selectivity of VOC to CO_2 (%);

C_{CO2} : CO_2 concentration of outlet flow at a temperature T (ppm).

3. Results and discussion

Catalyst characterization

The morphology and elemental distribution on the catalyst surface were analyzed using SEM-EDX. SEM images of the cordierite ceramic surface and the metal oxides supported on cordierite revealed differences before and after impregnation, as shown in Figure 3. Figure 3a displays the uneven, rough surface of the cordierite ceramic, containing grooves and lacking the presence of active crystals. After impregnation, metal

https://doi.org/10.62239/jca.2024.041

oxide crystals were observed on the cordierite (Figures 3b-3d), confirming the successful impregnation of active phases onto the cordierite support.

In contrast to $Cu_1Mn_2O_x$/Cordierite, the metal oxide catalysts on cordierite exhibited a tendency for crystal agglomeration, forming large clusters with non-uniform sizes. For the $Cu_1Mn_2O_x$/Cordierite catalyst (Figure 3d), small crystals were uniformly distributed on the surface. This demonstrates that doping with single metal oxides reduces crystal size, leading to a more homogeneous distribution and decreased crystal agglomeration.

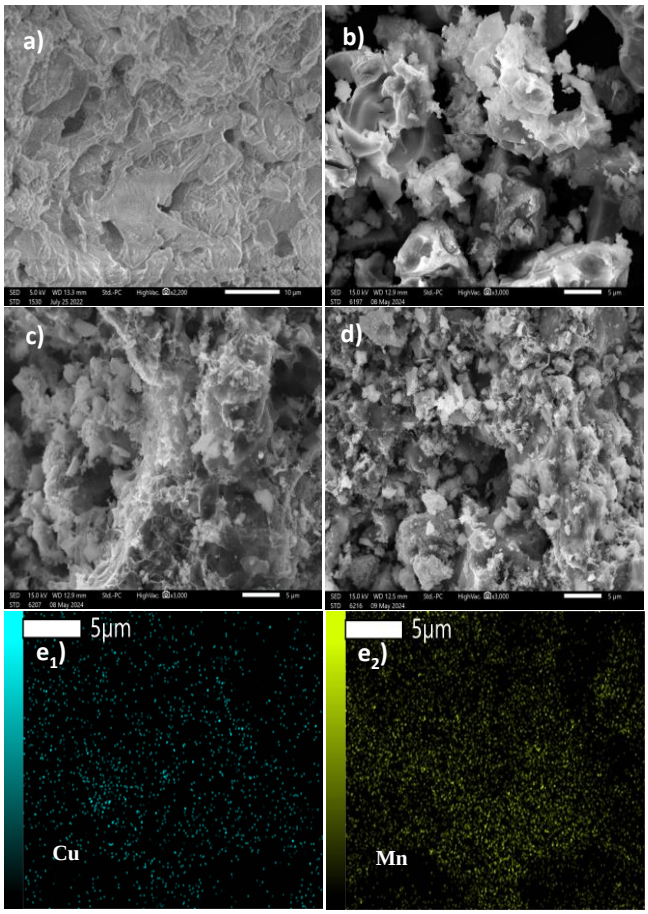

Fig. 1: SEM images of cordierite (a); CuO/Cordierite, MnO_2/Cordierite and $Cu_1Mn_2O_x$/Cordierite (b→d); Elemental mapping distribution of $Cu_1Mn_2O_x$ (e_1→e_2)

EDS elemental mapping revealed a homogeneous distribution of Cu and Mn on the $Cu_1Mn_2O_x$/Cordierite catalyst surface (Figure 1e), while single metal oxide catalysts showed poorer distribution , consistent with SEM images. The measured Mn Cu molar ratio of 2.07 for $Cu_1Mn_2O_x$ indicates a uniform distribution of Cu-Mn active components on the cordierite support, consistent with the precursor salt ratio used during preparation. The Cu-Mn active components were uniformly supported on the cordierite surface through the impregnation method.

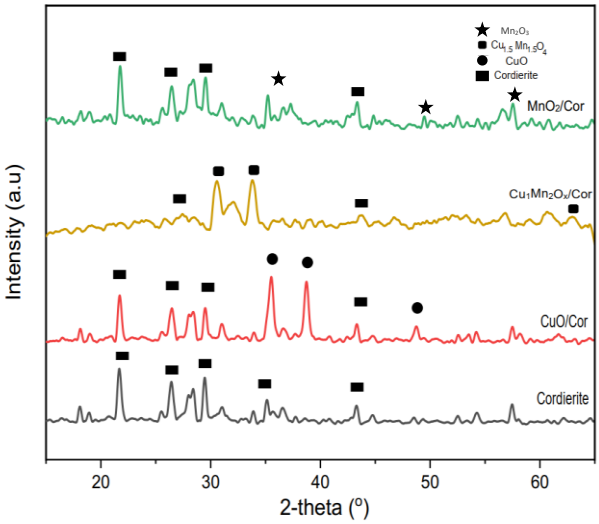

Fig. 2: X-ray diffraction spectra of cordierite

CuO/Cordierite, MnO_2/Cordierite and $Cu_1Mn_2O_x$/Cordierite

X-ray diffraction (XRD) analysis was employed to identify the phase structure and crystallite size of the catalysts. The XRD patterns (Figure 2) confirmed that the incorporation of active phase components did not alter the cordierite support structure, as evidenced by the presence of characteristic cordierite diffraction peaks. In the case of the $Cu_1Mn_2O_x$ catalyst supported on ceramic, diffraction peaks at 2θ values of 30.53°, 43.66°, and 57.74° were observed, corresponding to the (220), (400), and (333) crystal planes of the $Cu_{1.5}Mn_{1.5}O_4$ spinel structure [13]. This confirms the successful loading of the $CuMnO_x$ active phases onto the ceramic, with the spinel phase exhibiting characteristic XRD peaks. The absence of diffraction peaks for Mn oxide and CuO phases suggests the formation of a Cu-Mn solid solution with a spinel structure due to Cu doping into MnO_2. This doping-induced lattice distortion, arising from the size mismatch between Mn atoms (1.37 Å) and Cu^{2+} cations (0.73 Å) [16], creates crystal defects that facilitate VOCs oxidation by enhancing the mobility of surface oxygen species. The CuO/Cordierite sample displayed diffraction peaks at 2θ angles of 35.52°, 38.64°, and 48.8°, corresponding to the (002), (111), and (202) crystal planes of CuO [17], confirming the presence of the CuO phase. Furthermore, the XRD pattern of MnO_2 revealed the presence of bixbyite Mn_2O_3, with characteristic diffraction peaks at 2θ values of 32.9° (222), 49.16° (134), and 55.16° (440) [18].

The specific surface areas of $Cu_1Mn_2O_x$/Cordierite, CuO/Cordierite, and MnO_2/Cordierite were determined

https://doi.org/10.62239/jca.2024.041

to be 8.349, 3.06, and 1.56 m^2/g, respectively. The significantly higher surface area of $Cu_1Mn_2O_x$ is attributed to the synergistic Cu-Mn interaction, increasing surface defects and oxygen vacancies, leading to more active sites for enhanced oxygen adsorption and activation, thus improving VOCs oxidation.

Table 1: Characteristics of catalyst and ceramic specimens

Sample	S_{BET} (m^2/g)	$d_{crystal}$ (nm)	H_2 consumption (mmol/g)
$Cu_1Mn_2O_x$/cordierite	8.349	14,28	1.794
CuO/cordierite	3.06	22,86	1.143
MnO_2/cordierite	1.56	23,48	0.699
Cordierite	0.2	-	0

The larger surface area also facilitated better VOC-active site contact [13]. This is consistent with crystallitesize calculations, revealing $Cu_1Mn_2O_x$ had the smallest crystallite size, suggesting doping metal oxides increases defect density and reduces lattice size, leading to better dispersion on cordierite (supported by SEM and elemental mapping), thereby significantly enhancing the specific surface area.

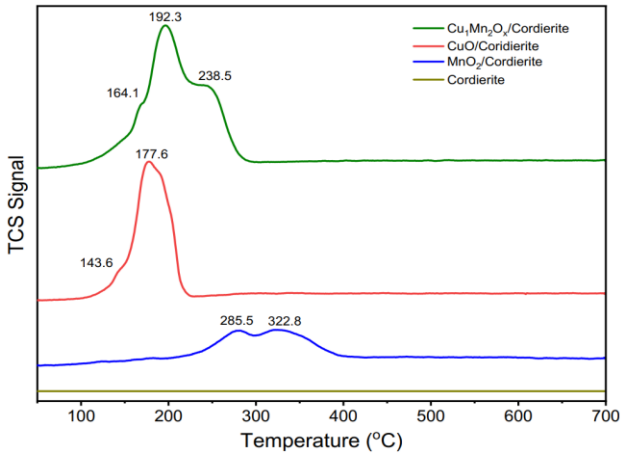

Fig. 3: H_2-TPR profiles of cordierite, MnO_2/Cordierite, CuO/ Cordierite and $Cu_1Mn_2O_x$/ Cordierite samples

The redox capability and oxygen mobility of the catalysts were investigated using temperature-programmed reduction (H_2-TPR). For CuO/Cordierite, the reduction peak observed at 143.6°C corresponds to the reduction of Cu^{2+} to Cu^+, while the peak at 177.6°C is ascribed to the reduction of Cu^+ to Cu^0 or the reduction of well-dispersed Cu^{2+} species present on the ceramic surface to Cu^0 [19]. The TPR-H_2 profile of MnO_2/Cordierite reveals two distinct reduction events: the initial peak at 285.5°C corresponds to the reduction of MnO_2 to Mn_2O_3, while the subsequent peak at 322.8°C is attributed to the reduction of Mn_2O_3 to Mn_3O_4 [20].

For the $Cu_1M_2nO_x$/Cordierite catalyst, the two reduction peaks observed at higher temperatures can be attributed to the reduction of copper and manganese species, respectively [19]. Meanwhile, the reduction peak at the lower temperature of 164°C is ascribed to the reduction of surface chemisorbed oxygen species on the Cu-Mn oxide, the presence of which promotes catalytic activity [21]. The shift of reduction peaks to lower temperatures in mixed metal oxides compared to single metal oxides is attributed to increased lattice defects and oxygen vacancies, enhancing oxygen mobility and catalytic activity. Doping also reduces crystallite size, increasing surface area and promoting active phase dispersion, facilitating H_2-metal oxide contact and easier reduction. Cordierite, assessed via TPR, remained stable below 800°C. $Cu_1Mn_2O_x$/Cordierite showed the highest H_2 consumption, indicating abundant mobile lattice oxygen. Despite lower temperature reduction peaks, CuO/Cordierite consumed less H_2. MnO_2, with Mn^{4+} ions, has ample lattice oxygen but lower consumption due to limited mobility. $Cu_1Mn_2O_x$ has more lattice oxygen than CuO and greater mobility than MnO2.

Catalytic performance of VOCs oxidation

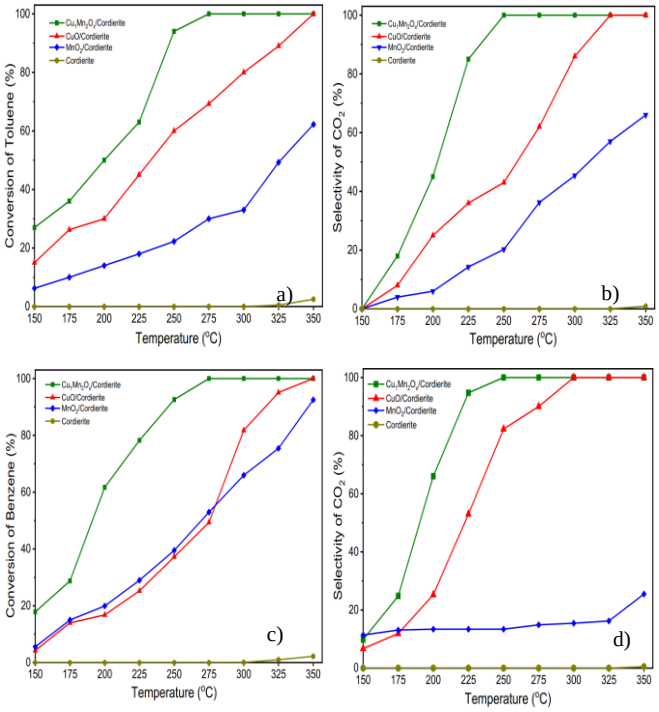

Fig. 4: Conversion for toluene (a) and selectivity of CO_2 (b). Conversion for benzene (c) and selectivity of CO_2 (d)

The catalytic activity for benzene and toluene oxidation was evaluated at concentrations of 7000 ppm and

12000 ppm, respectively. Cordierite ceramic was used to assess the thermal stability of VOCs and exhibited negligible conversion (<5%) at 350°C, confirming its inertness towards VOC oxidation under the reaction conditions. In general, mixed metal oxide catalysts exhibit higher conversion and CO_2 selectivity compared to single metal oxides at the same temperature. The $Cu_1Mn_2O_x$/Cordierite catalyst demonstrated the highest activity for both toluene and benzene, achieving complete oxidation to CO_2 at 275°C and T_{90}= 243°C, 246°C for toluene and benzene, respectively. These temperatures are 71°C and 101°C lower than those observed for the pure CuO and MnO_2 bulk catalysts in toluene oxidation. The superior catalytic activity of $Cu_1Mn_2O_x$/Cordierite can be attributed to the well-dispersed elements on the ceramic support surface, leading to increased reaction sites for toluene and benzene interaction. Additionally, the enhanced redox capability and high oxygen vacancy concentration due to the modification of single metal oxides into mixed metal oxides through the formation of solid solutions and crystal defects [11-13] contribute to the improved performance. The catalytic activity of monolithic CuMnOx was comparable (T90 = 248 °C) to that of powder catalysts prepared by more complex methods, and superior to other ceramic-supported catalyst systems (1000 ppm toluene, T90 = 263 °C) [14, 15].

Stability of catalyst

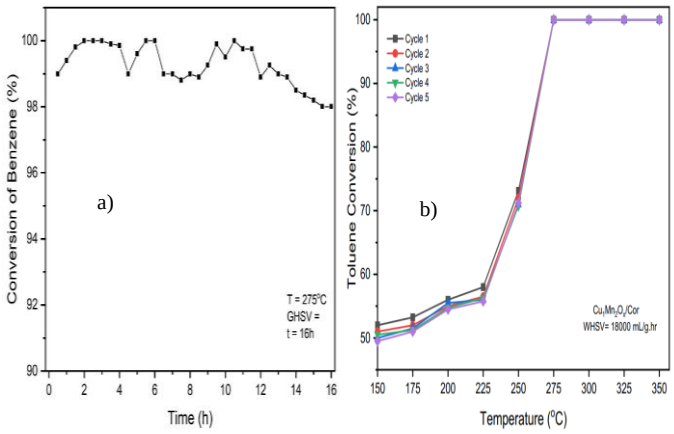

Fig. 5: Assessment of stability (a) and recyclability of the $Cu_1Mn_2O_x$/Cordierite (b)

The $Cu_1Mn_2O_x$/Cordierite catalyst exhibited excellent stability, maintaining high toluene conversion (98%) over 16 hours of continuous operation at 275°C. Additionally, the catalyst demonstrated good reusability, achieving complete toluene oxidation in five consecutive cycles with a reaction velocity (WHSV) of about 18,000 mL/(g•hr) and pollutant concentrations of 7000 ppm, albeit with a minor decrease in conversion after each cycle. The cordierite support played a crucial role in enhancing the catalyst's stability, thermal resistance, and mechanical durability, contributing to its sustained activity and reusability, making it a promising candidate for industrial applications.

4. Conclusion

In this study, $Cu_1Mn_2O_x$ catalyst was successfully synthesized via a simple impregnation method, achieving high and uniform dispersion on the Cordierite surface. The formation of a stable $Cu_{1.5}Mn_{1.5}O_4$ spinel structure on the cordierite support was confirmed by SEM-EDX and XRD results. The incorporation of Cu into MnO_2 enhanced the mobility of surface oxygen species, as demonstrated by the shift of reduction temperatures towards lower values and increased H_2 consumption. The $Cu_1Mn_2O_x$/Cordierite catalyst exhibited the highest activity, achieving 100% conversion at 275°C for the treatment of high-concentration aromatic compounds ($C_{toluene}$ = 7000 ppm, $C_{benzene}$ = 12000 ppm) at a high space velocity (WHSV = 18000 ml/g.hr). The catalyst demonstrated good stability and reusability, making it a promising candidate for industrial applications in the catalytic treatment of volatile organic compounds.

Acknowledgments

This work has been supported by the RoHan Project funded by the German Academic Exchange Service (DAAD, No. 57315854) and the Federal Ministry for Economic Cooperation and Development (BMZ) inside the framework "SDG Bilateral Graduate school programme".

References

1. Park, J. H., Goldstein, A. H., Timkovsky, J., Fares, S., Weber, R., Karlik, J., & Holzinger, R. (2013). Science, 341(6146), 643-647. https://doi.org/10.1126/science.1235053
2. Adebayo, B. O., Trautman, J., Al-Naddaf, Q., Rownaghi, A. A., & Rezaei, F. (2021)., 55(13), 9255-9265. https://doi.org/10.1021/acs.est.1c00912
3. G. Liu, K. Yang, J. Li, W. Tang, J. Xu, H. Liu, R. Yue, Y. Chen, J. Phys. Chem. C 118 (2014) 22719–22729. https://doi.org/10.1021/jp501434f
4. Liotta, L.F., Wu, H., Pantaleo, G., Venezia, A.M., 2013. Catal. Sci. Technol. 3, 3085–3102. https://doi.org/10.1039/C3CY00193H
5. Wang X, Liu Yi, Zhang Y, Zhang T, Chang H, Zhang Y, et al. Appl Catal B 2018;229:52–62. https://doi.org/10.1016/j.apcatb.2018.02.007

6. Wang, X., Liu, Y., Zhang, Y., Zhang, T., Chang, H., Zhang, Y., & Jiang, L. (2018). Applied Catalysis B: Environmental, 229, 52-62. https://doi.org/10.1016/j.apcatb.2018.02.007
7. Luo M, Cheng Y, Peng X, Pan W. Chem Eng J 2019;369:758–65. https://doi.org/10.1016/j.cej.2019.03.056
8. Chen J, Chen Xi, Xu W, Xu Z, Chen J, Jia H, et al. Chem Eng J 2017;330:281–93. https://doi.org/10.1016/j.cej.2017.07.147
9. Zhou, X., Lai, X., Lin, T., Feng, J., Hou, Z., Chen, Y., 2018. New J. Chem. 42,16875–16885. https://doi.org/10.1039/C8NJ02908C
10. Tang, W., Wang, S., Xiao, W., Du, S., Lu, X., Hoang, S., et al., 2019. Catal. Today 320, 196–203. https://doi.org/10.1016/j.cattod.2017.10.045
11. Yang, Y., Si, W., Peng, Y., Chen, J., Wang, Y., Chen, D., ... & Li, J. (2024). Applied Catalysis B: Environmental, 340, 123142. https://doi.org/10.1016/j.apcatb.2023.123142
12. Xia, Y., Yang, Y., Li, M., Lan, Z., Chu, Y., Wu, G., ... & Chen, Y. (2024). Separation and Purification Technology, 126993. https://doi.org/10.1016/j.seppur.2024.126993
13. Xu, Y., Qu, Z., Ren, Y., & Dong, C. (2021). Applied Surface Science, 560, 149983. https://doi.org/10.1016/j.apsusc.2021.149983
14. Yang, Y., Si, W., Peng, Y., Chen, J., Wang, Y., Chen, D., ... & Li, J. (2024). Applied Catalysis B: Environmental, 340, 123142. https://doi.org/10.1016/j.apcatb.2023.123142
15. Yuhang, D. A. I., Kaige, L. I., Jinxian, Z. H. A. O., Jun, R. E. N., & Yanhong, Q. U. A. N. (2024). Journal of Fuel Chemistry and Technology, 52(1), 55-64. https://doi.org/10.1016/S1872-5813(23)60381-0
16. Zhou, M., Cai, L., Bajdich, M., García-Melchor, M., Li, H., He, J., & Zheng, X. (2015). ACS Catalysis, 5(8), 4485-4491. https://doi.org/10.1021/acscatal.5b00488
17. D. Zhu, L. Wang, W. Yu, H. Xie, Scientific reporters 8 (2018). https://doi.org/10.1038/s41598-018-23174-z
18. L. Chen, T. Zhang, H. Cheng, Ryan M. Richards, Z.Qi, Nanoscale 12 (2020) 17902-179144. https://doi.org/10.1039/D0NR04738D
19. M. Morales, B. Barbero, L. Cadus, Appl. Catal. B 67 (2006) 229–236. https://doi.org/10.1016/j.apcatb.2006.05.006
20. S. Todorova, H. Kolev, J.P. Holgado, G. Kadinov, C. Bonev, R. Pereíguez, A.Caballero, Applied Catalysis B: Environmental, 94 (2010) 46-54. https://doi.org/10.1016/j.apcatb.2009.10.019
21. W. Tang, X. Wu, S. Li, X. Shan, G. Liu, Y. Chen, Appl. Catal. B 162 (2015) 110–121. https://doi.org/10.1016/j.apcatb.2014.06.030